Exploring the dynamics of dimer crossing over a Kramers type potential

Mesfin Asfaw and Yohannes Shiferaw

Citation: J. Chem. Phys. **136**, 025101 (2012); doi: 10.1063/1.3675920
View online: http://dx.doi.org/10.1063/1.3675920
View Table of Contents: http://jcp.aip.org/resource/1/JCPSA6/v136/i2
Published by the American Institute of Physics.

Exploring the dynamics of dimer crossing over a Kramers type potential

Mesfin Asfaw[a] and Yohannes Shiferaw
Department of Physics and Astronomy, California State University Northridge, California 91330, USA

(Received 14 October 2011; accepted 20 December 2011; published online 10 January 2012)

We explore the escape rate of a dimer crossing a potential barrier using both analytical and numerical approaches. We find that for small coupling strength k, the barrier hopping can be well approximated by a two step reaction scheme where one monomer hops over the barrier and is then followed by the other. In this regime the escape rate increases with k showing that the cooperativity between monomers enhances the crossing rate. However, in the limit of large coupling strength, applying the method of adiabatic elimination, we find that the escape rate is a decreasing function of k. Thus, we find that the escape rate is a non-monotonic function of the spring constant which is peaked at an optimal coupling strength. Furthermore, in the presence of a weak periodic signal, we show that the system response to the periodic signal is pronounced at a particular spring constant showing the dimer can be transported rapidly across the reaction coordinate in a half period. © *2012 American Institute of Physics*. [doi:10.1063/1.3675920]

I. INTRODUCTION

Studying the statistical behavior of biological and soft matter systems such as polymers and membranes is vital and has diverse applications in various disciplines.[1,3–6] However, their transport and response properties are difficult to understand since they are multicomponent systems with features that depend on their size, flexibility, and shape. In the last few decades considerable attention has been given to understand the thermally activated escape rate of polymers trapped in a potential well.[7–12] In particular Sebastian *et al.*[2] and Sung *et al.*[3,4] computed the crossing rate of a polymer as a function of the number of monomers, and the strength of interaction between individual monomers. They found that indeed the escape rate was a nontrivial function of these parameters. In particular, they found that the crossing rate was a nonmontonic function of the force between monomers, so that at an optimal interaction strength the crossing rate was maximized. This result is important since it implies that the thermally driven escape rate of complex molecules can potentially be altered by varying the interactions between the individual components. This work is supported by studies of simplified two particle systems which show that their transport properties are typically non-monotonic functions of system parameters.[13–17]

In this paper we will study, using both numerical and analytical techniques, the thermally activated escape rate of two interacting monomers (a dimer) that cross a potential barrier. Our aim is to understand how the crossing rate depends on system parameters such as temperature, barrier height, and especially the interaction strength between the monomers. A basic motivation for this study is to develop a simple model where the transport properties of a multicomponent system can be explored in detail. Furthermore, this study has direct applications to a variety of biologically relevant macromolecules. For instance, Kinesin, a tiny molecular motor responsible for transporting vesicles in the cytoplasm of cells, has two structurally similar heads, where each head contains a binding site for an ATP molecule.[18] Remarkably, Kinesin interacts with microtubule filaments in such a way to induce a biased random walk. To date a great deal of work has been done to understand the basic transport properties of Kinesin at a phenomenological level. However, it is not understood in detail how these transport properties depend on the structure of Kinesin, the external forces on the molecule, and especially on the interaction strength of the Kinesin heads. The model considered here will serve as a starting point from which to understand these more complex features.

An important property of dimers and polymers is their response to external forces. In particular, considerable work has been done on the phenomenon of stochastic resonance where the escape rate of a single Brownian particle can be enhanced by a subtle interplay between a periodic driving force and noise.[19–22] Also, the stochastic resonance of two particle systems diffusing along a one-dimensional periodic substrate has been explored in detail.[23] Recently, we studied the stochastic resonance of a flexible polymer surmounting a bistable potential.[10,11] Our numerical and analytical analysis showed that the effect of stochastic resonance can be maximized at a particular chain length, and also by fine tuning the interaction strength between monomers. In the present study, we will also explore the response of a dimer to a periodic external force. Again, our goal will be to understand the interaction between conformation and noise in a simple yet nontrivial context.

In this work, we consider a dimer with two monomers that interact via harmonic springs with a force constant k. Our approach will be first to explore the escape dynamics of the dimer using a direct numerical simulation of the Brownian dynamics. We then use insights from our numerical simulations to motivate a simple phenomenological model of the crossing rate for small k. Using this approach we show that there exists an optimal force constant, denoted by k_{opt}, at which the crossing rate of the dimer is maximized. For large k we exploit the fact that the center of mass (CM) motion is much slower than the relative motion to apply the method of adiabatic

[a] Electronic mail: mesfin.taye@csun.edu.

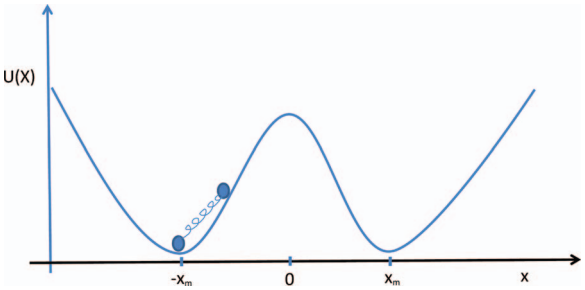

FIG. 1. Schematic diagram for a dimer walking on Kramers potential. The potential wells and the barrier top are located at $x = \pm x_m$ and $x = 0$, respectively. The dimer is initially situated at $x = -x_m$. The dimer crosses the barrier assisted by the thermal background kicks and its conformational change along the reaction coordinate.

elimination. Using this approach we show that strong coupling decreases the escape rate of a dimer. Finally, we consider the response of the dimer to a periodic external force. Our main finding here is that the signal-to-noise ratio (SNR) exhibits a pronounced peak at an optimal noise and coupling strength.

II. THE MODEL

In this study, we model a dimer as a system of two monomers which interact via a harmonic force. The rest length between the two monomer l is assumed to be much less than the potential width $2x_m$, $l \ll 2x_m$ where x_m denotes the position of the potential minima. Each monomer experiences a friction coefficient γ and is placed in a Kramers potential as shown in Fig. 1. The dynamics of the two beads is governed by the Langevin equation,

$$\gamma \frac{dx_1}{dt} = -k(x_1 - x_2) - \frac{\partial U(x_1)}{\partial x_1} + \xi_1(t), \tag{1}$$

$$\gamma \frac{dx_2}{dt} = -k(x_2 - x_1) - \frac{\partial U(x_2)}{\partial x_2} + \xi_2(t), \tag{2}$$

where k is the spring (elastic constant) of the dimer. The random force $\xi_n(t)$ is considered to be Gaussian and white noise satisfying

$$\langle \xi_n(t) \rangle = 0, \quad \langle \xi_n(t)\xi_n(t+\tau) \rangle = 2D\gamma\delta(\tau), \tag{3}$$

where $D = k_B T$ is the strength of the thermal noise. The external potential energy is given by

$$U(x) = -\left(\frac{\omega_B^2}{2}\right)x^2 + \frac{1}{4}\left(\frac{\omega_B^2}{x_m^2}\right)x^4, \tag{4}$$

as shown in Fig. 1. The potential minima are located at $x = \pm x_m$, while the barrier of height $U_B = x_m^2\omega_B^2/4$ is centered at $x = 0$. The parameter $\omega_B^2 = (1)/(2)\omega_0^2$ and ω_0^2 designates the potential curvatures of the barrier top and the well minima, respectively.

Let us now introduce a dimensionless time $\bar{t} = t/\tau$ where $\tau = \gamma x_m^2/U_B$, rescaled length $\bar{x}_{1,2} = x_{1,2}/x_m$, rescaled noise strength $\bar{D} = D/U_B$, rescaled coupling constant $\bar{k} = k/\omega_B^2$, and dimensionless Gaussian white noise $\bar{\xi}_{1,2} = \xi_{1,2}(t)x_m/U_B$. Hereafter for simplicity the bar will be dropped. Equations (1) and (2) can be rewritten in terms of the rescaled parameters

$$\frac{dx_1}{dt} = -4k(x_1 - x_2) - \frac{\partial U(x_1)}{\partial x_1} + \xi_1(t), \tag{5}$$

$$\frac{dx_2}{dt} = -4k(x_2 - x_1) - \frac{\partial U(x_2)}{\partial x_2} + \xi_2(t), \tag{6}$$

where $\partial U(x_1)/\partial x_1 = -4(x_1 - x_1^3)$ and $\partial U(x_2)/\partial x_2 = -4(x_2 - x_2^3)$. One can note that

$$\langle \xi_n(t) \rangle = 0, \quad \langle \xi_n(t)\xi_n(t+t') \rangle = 2D\delta(t'), \tag{7}$$

where D is now a dimensionless parameter. In this study we will also consider the dynamics of the CM located at $x_{cm} = (x_1 + x_2)/2$, and the relative motion $y = (x_2 - x_1)/2$ of the dimer.

III. NUMERICAL SIMULATION AND COMPUTATIONAL MECHANICS

In this section, we explore the escape rate of a dimer trapped in a potential well using Brownian dynamics simulations. Our approach is to solve Eqs. (5) and (6) by solving the corresponding set of discrete Langevin equations. As a starting point we will first analyze the trajectory of the center of mass x_{cm}, along with the relative motion y of the two monomers. In Figs. 2 and 3 we plot the typical trajectories

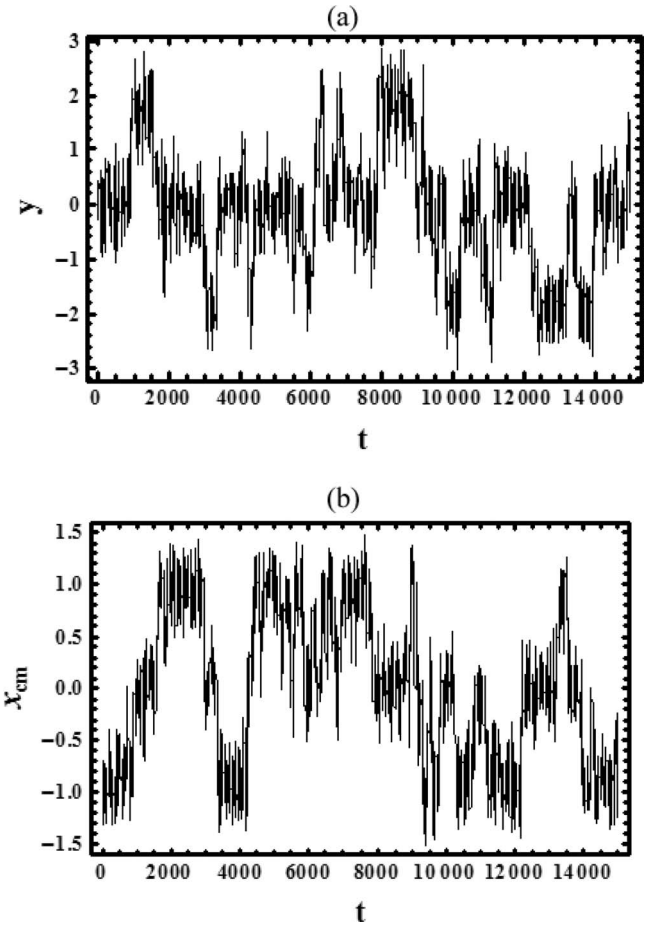

FIG. 2. (a) The trajectory for the relative motion versus time. (b) The snapshot showing the trajectory for the center of mass as a function of t for $D = 0.5$ and $k = 0.001$. Both y and x_{cm} cross the potential barrier frequently showing they have a comparable escape rate.

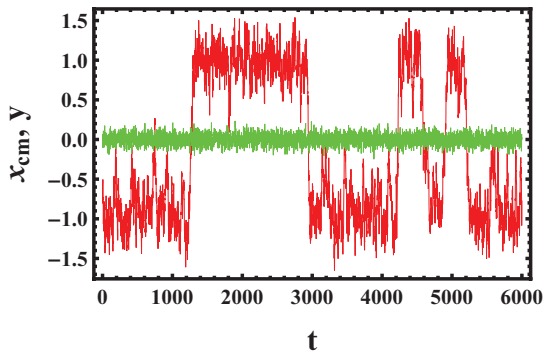

FIG. 3. The trajectory for the relative motion (green) and the center of mass (red) as a function versus time for a given $D = 0.5$ and $k = 5.0$. The relative motion fluctuates around the potential minima while the center of mass motion rarely crosses the potential barrier.

for the x_{cm} and y for small and large k, respectively. Our main observation is that there is a distinct qualitative change in the escape dynamics as the coupling strength is increased. In particular, for small k, we notice that the CM spends much of its time at three positions: $x_{cm} = -1$, which corresponds to both monomers trapped in the left well. $x_{cm} = 0$, where one monomer is at $x_m = -1$ and the other at $x_m = +1$, and finally $x_{cm} = 1$, where both monomers have escaped to the well at $x_m = +1$. Furthermore, the transition rate of the CM from these distinct states is roughly the same as transitions of the relative coordinate y. This result implies that the motion of the CM is similar to the relative motion. On the other hand, in the limit of large k (see Fig. 3) the relative position of the monomers changes rapidly, but with an amplitude that is much smaller than the distance between minima. Also, we notice that the CM makes transitions between minima on a time scale that is much longer than the fluctuations of the relative motion. In a later section, we will exploit this difference in time scales to apply a systematic adiabatic elimination method valid in the limit of large k. Overall, these numerical simulations show that the escape dynamics is crucially dependent on the strength of coupling of the two monomers.

To analyze this dependence further we have computed the escape rate of a dimer as a function of the strength of coupling k. To compute this quantity we note that the escape rate is just the inverse of the first passage time (MFPT) of the CM as it goes from $x_m = -1$ to $x_m = +1$. We compute the MFPT by averaging over 10^6 independent simulation runs. In Fig. 4(a) we plot the escape rate as a function of the coupling strength k, for fixed parameters $D = 1$ and $D = 0.5$. Figure 4(b) exhibits the rate as a function of k for $D = 2$. Here, we see that the escape rate is a nonmonotonic function of k with a peak at an optimal coupling strength k_{opt}. To gain a deeper insight into this finding we have also computed the effective potential $V^{eff}(x_{cm})$ defined as $P(x_{cm}) = \exp[(-V^{eff}(x_{cm}))/k_BT]/C$, where $P(x_{cm})$ is the probability distribution of the position of CM, and where C is a normalization constant. The effective potential as function of x_{cm} is plotted in Fig. 5(b) for small and large coupling k. The figure shows that the effective potential is a triple-well potential for small k with minima at $x_{cm} = -1$, $x_{cm} = 0$, and $x_{cm} + 1$. Now for $k = 0.001$ we find that the global minima occurs at $x_{cm} = 0$. However, as k is increased

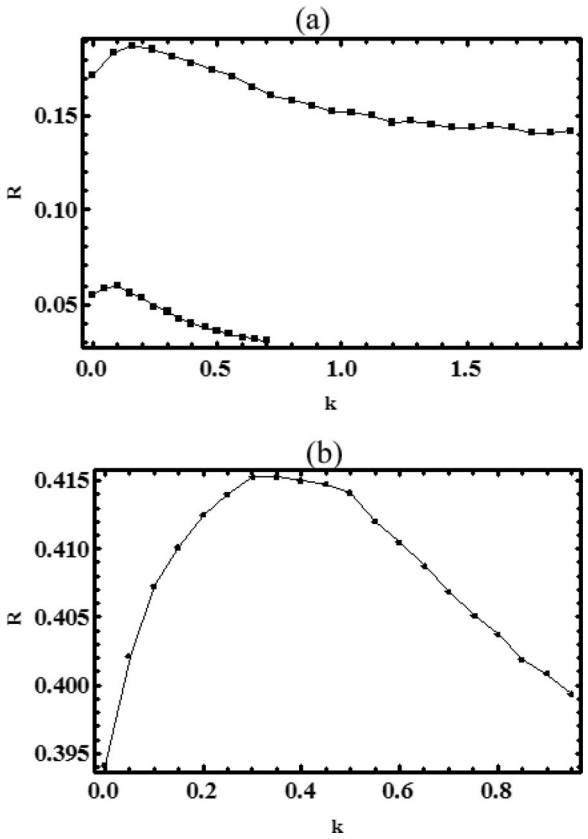

FIG. 4. (a) The dependence of R as a function of coupling constant k for noise strength $D = 1.0$ and $D = 0.5$ from top to bottom. The figure shows that R attains a maximum value at an elastic constant k_{opt}. The optimal coupling constant shifts to the right as D increases. (b) The escape rate R as a function of k for parameter choice $D = 2.0$.

the depth of this well decreases so that eventually the CM is most likely to be found at $x_{cm} = \pm 1$. Now, increasing k even further to $k = 1$ (Fig. 6) shows that the central well disappears, and that the CM is now governed by a bistable potential. This occurs since the coupling strength is so large that it is unlikely for the monomers to reside in different wells.

The main insight from our numerical simulations is that for small k our system can be essentially treated as a three state system. Now as k is increased further then this three state feature is lost and our dimer effectively behaves as a single particle in a bistable potential. In Sec. IV we will exploit the simplicity of the three state feature, valid for small k, to analytically compute the escape rate as a function of system parameters. On the other hand, for large k we take advantage of the separation of time scales to eliminate adiabatically the relative dynamics. Our analytical results can then be used to compute the precise value of k which maximizes the escape rate of the dimer.

IV. QUANTITATIVE ANALYSIS FOR THE CROSSING RATE IN THE WEAK COUPLING REGIME

Our Brownian dynamics simulations revealed that in the limit of small k the CM crosses from one well to the other via a two step process. Given that the two monomers are initially trapped in the well located at $x_m = -1$, then after some time one monomer hops over the barrier and is then followed by

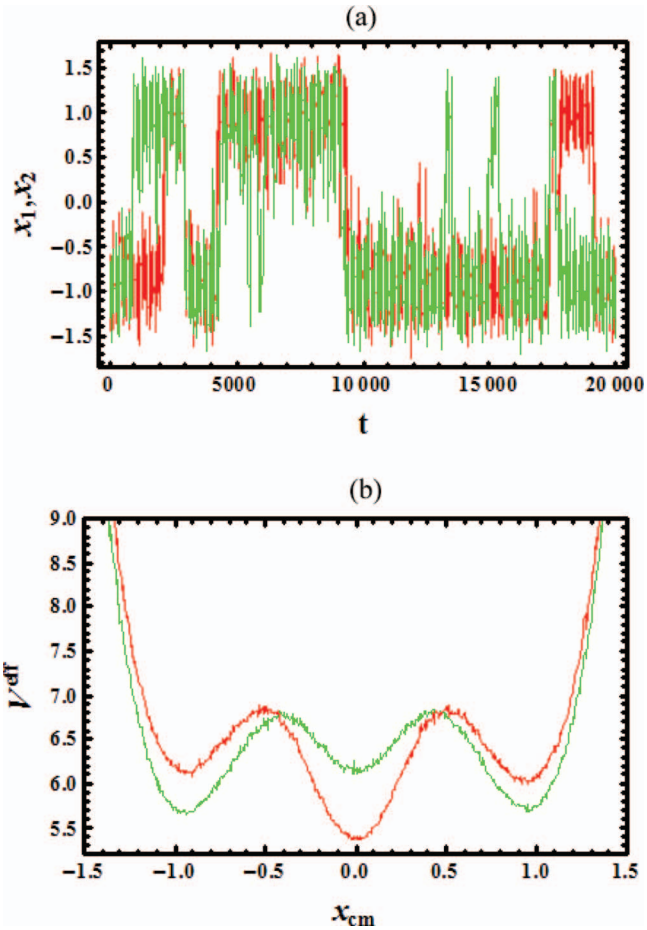

FIG. 5. (a) The trajectory for each monomers versus time; first monomer x_1 (green) and second monomer x_2 (red) for a given $D = 0.5$ and $k = 0.001$. (b) The effective potential as a function of x_{cm}. The red line corresponds to $k = 0.001$ while the green line for $k = 0.5$. As k increases, the depth of the central well decreases.

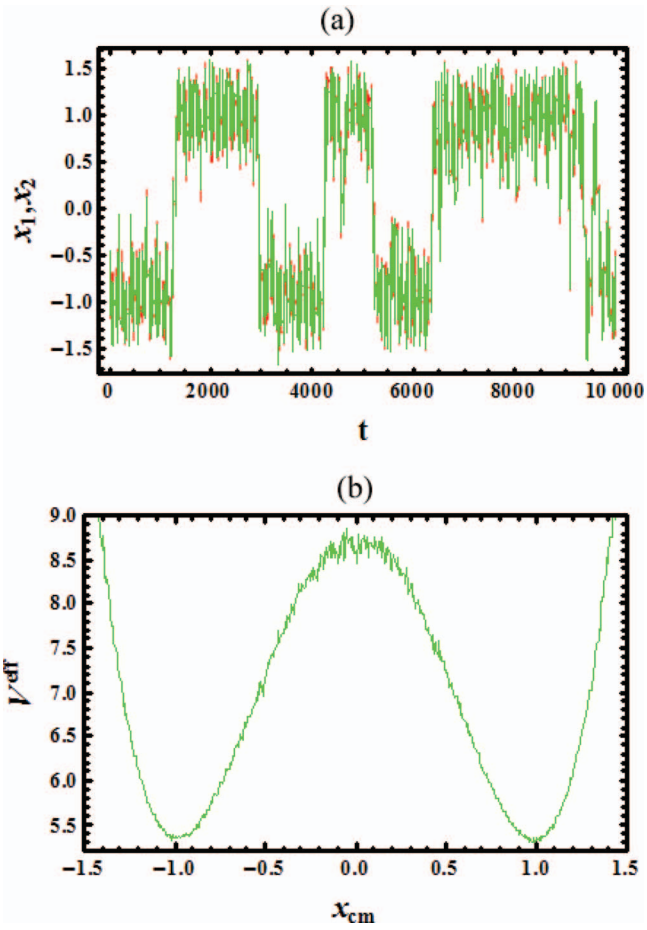

FIG. 6. (a) The snapshots showing the trajectory each monomers as a function of time; first monomer x_1 (green) and second monomer x_2 (red) for a given $D = 0.5$ and $k = 1$. (b) The effective potential as a function of x_{cm} for fixed $k = 1$. As k increases the potential-well at $x_{cm} = 0$ shifts upwards.

the other. Thus, as shown using the numerical simulations (see Fig. 5(b)), the effective potential for the CM has three minima located at -1, 0, $+1$, and barrier crossing occurs due to two discrete transitions from -1 to 0 followed by 0 to $+1$.

In small k regime, the problem can be mapped into a single Brownian particle hopping along the effective triple-well potential. The forward rate from -1 to 0 is denoted as R_1 and its backward rate as R_3. R_2 is the forward crossing rate from 0 to 1. In this work, we assume that the dimer jumps directly from one minima to the other minima (between the three states -1, 0, $+1$) as shown in Fig. 7. The three state approach is valid in high barrier limit approximation.

We take advantage of this simplified picture by deriving an effective dynamics of this two step system. To do so we first approximate the transition rate of the first step by pining the position of one monomer at $x_1 = -1$ and letting the other at position x_2 undergo a thermally activated barrier crossing. To describe this dynamics we write the effective potential of the free monomer as

$$U^{eff}(x_2) = 4kx_2 + 2(k-1)x_2^2 + x_2^4. \tag{8}$$

Note here that since the monomer at x_1 is pinned then x_2 needs to hop over a larger potential barrier due to the attractive force between the two monomers. In the high barrier limit we can estimate the crossing rate as

$$R_1 \approx 2\frac{\sqrt{|\omega_0||\omega_{x'_m}|}}{2\pi} e^{\frac{-\Delta V_e}{D}}, \tag{9}$$

where ΔV_e denotes the barrier height of the effective potential, and where ω_0 and $\omega_{x'_m}$ denote the curvatures at the barrier top and the well minima, respectively. Note here that we have included a factor of 2 since either monomer can make the

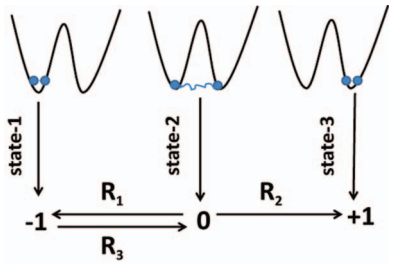

FIG. 7. The three state scheme. R_1 and R_3 denote the forward rate from -1 to 0 and the rate from 0 to -1, respectively. R_2 is the forward crossing rate from 0 to 1. There are three conformational states denoted as state-1 when the two particles situated at -1, state-2 when the two particles positioned at different wells, and state-3 if the two particles located at 1.

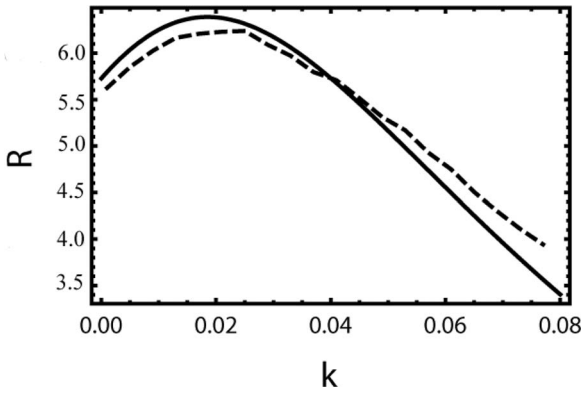

FIG. 8. The rate R as a function of k for parameter choice $D = 0.15$. The solid line depicts the rate evaluated analytically from our simple model, while the dashed line indicates the rate from the numerical simulations.

barrier crossing. The transition rate can be computed directly which yields the result that

$$R_1 = \frac{2\sqrt{2}}{\pi} e^{\eta}((2+k)^2(-1+3\sqrt{1-4k}+4k)^2)^{1/4}, \quad (10)$$

where $\eta = -(1+\sqrt{1-4k}+10k-4\sqrt{1-4k}k-2k^2)/2D$. The rate R_1 decreases monotonically as a function of k. Now once one monomer has transitioned to the well at $x = +1$, then the monomer which remained at $x = -1$ can itself hop the barrier. To compute the transition rate of this event we compute the effective potential felt by this monomer as

$$U^{eff}(x_1) = -4kx_1 + 2(k-1)x_1^2 + x_1^4. \quad (11)$$

The crossing rate of the monomer at $x = -1$ is then computed, using Eq. (9), as

$$R_2 = e^{-\frac{(1-4k)^{3/2}}{D}}((-2+7k+4k^2)^2)^{1/4}\frac{2}{\pi}, \quad (12)$$

which increases monotonically as a function of k. These computations determine the forward rates R_1 and R_2 of the three state reaction scheme and also the backward rate $R_3 = R_2$ since these transitions are identical. To compute the full reaction rate from state -1 to $+1$ we follow Goldhirsch and Gefen[24,25] who find that the full reaction rate is $R = R_1R_2/(R_1 + R_2 + R_3) = R_1R_2/(R_1 + 2R_2)$. Computing this reaction rate and plotting R as a function of k reveals that the reaction is nonmonotonic with a peak at an optimal value of k_{opt} as shown in Fig. 8. As depicted in the same figure, the rate from our simplified model matches remarkably well with our numerical results.

V. EXPLORING THE THERMALLY ACTIVATED RATE VIA THE ADIABATIC ELIMINATION METHOD

For small k, we examined how the crossing rate behaves as a function of the different model parameters in Secs. III and IV. In this section, we rather explore the dynamics for the dimer employing the adiabatic elimination method. In the limit of large k, the center of mass motion of the dimer is significantly slow compared to the relative motion of the dimer. Hence, one can eliminate the fast changing variable. To begin with, let us now write the corresponding Fokker–Planck equation for the Langevin equations (5) and (6) which can be written in terms of the probability density $P(x_1, x_2, t)$ as

$$\frac{\partial}{\partial t}P(x_1,x_2,t) = \frac{\partial}{\partial x_1}\left(4k(x_1-x_2) + \frac{\partial U(x_1)}{\partial x_1} + D\frac{\partial}{\partial x_1}\right) \times P(x_1,x_2,t) + \frac{\partial}{\partial x_2}\left(4k(x_2-x_1) + \frac{\partial U(x_2)}{\partial x_2} + D\frac{\partial}{\partial x_2}\right)P(x_1,x_2,t) \quad (13)$$

Equation (13) can be rewritten in terms of the relative and center of mass coordinates as

$$\frac{\partial}{\partial t}P(x_{cm},y,t) = \frac{\partial}{\partial x_{cm}}\left(A(x_{cm},y) + \frac{D}{2}\frac{\partial}{\partial x_{cm}}\right)P(x_{cm},y,t) + \frac{\partial}{\partial y}\left(-kB(y,x_{cm}) + \frac{D}{2}\frac{\partial}{\partial y}\right)P(x_{cm},y,t) \quad (14)$$

where the parameters $A(x_{cm}, y) = (4x_{cm}[x_{cm}^2 - 1 + 3y^2])$ and $B(y, x_{cm}) = -y(16 + 8[3x_{cm}^2 - 1 + y^2]/k)$.

Defining a new rescaled quantity $\bar{y} = \sqrt{k}y$ and hereafter ignoring the bar, one can rewrite the above Fokker–Planck equation in terms of x_{cm} and y as

$$\frac{\partial}{\partial t}P(x_{cm},y,t) = \frac{\partial}{\partial x_{cm}}\left(A'(x_{cm},y) + \frac{D}{2}\frac{\partial}{\partial x_{cm}}\right)P(x_{cm},y,t) + k\frac{\partial}{\partial y}\left(-B'(y,x_{cm}) + \frac{D}{2}\frac{\partial}{\partial y}\right)P(x_{cm},y,t) \quad (15)$$

where $A'(x_{cm}, y) = (4x_{cm}[x_{cm}^2 - 1 + 3y^2/k])$ and $B'(y, x_{cm}) = -y(16 + 8[3x_{cm}^2 - 1 + y^2/k]/k)$. By tracing out the y degree of freedom, one can project $P(x_{cm}, y, t)$ into $P(x_{cm}, t)$; i.e, $P(x_{cm}, t) = \int P(x_{cm}, y, t)dy$. Let us now expand $P(x_{cm}, y, t)$ as

$$P(x_{cm},y,t) = \sum_n P_n(x_{cm},t)\psi_n(y,x_{cm}), \quad (16)$$

where $\psi_n(y, x_{cm})$ is the eigenfunction of

$$-\frac{\partial}{\partial y}B'(y,x_{cm})\psi_n(y,x_{cm}) + \frac{1}{2}D\frac{\partial^2}{\partial y^2}\psi_n(y,x_{cm}) = -\lambda_n\psi_n(y,x_{cm}). \quad (17)$$

The eigenvalue $\lambda_0 = 0$ and $\lambda_n > 0$ for $n \neq 0$. In the Appendix, we briefly revised the adiabatic elimination method which is formulated employing the eigenfunction expansion method.[26,27] Applying the adiabatic elimination method that is discussed in the Appendix, the effective Fokker–Planck equation for the slow dynamics is given by

$$\frac{\partial}{\partial t}P_0(x_{cm},t) = \left\{\frac{\partial}{\partial x_{cm}}\int A'(x_{cm},y)\psi_0(y,x_{cm})dy\right\} \times P_0(x_{cm},t) + \frac{1}{2}D\frac{\partial^2}{\partial x_{cm}^2}P_0(x_{cm},t). \quad (18)$$

The Langevin representation of the Fokker Planck equation (18) has a simple form

$$\frac{dx_{cm}}{dt} = -\Xi + \xi_{cm}(t) = -\frac{dV^{eff}(x_{cm}, y)}{dx_{cm}} + \xi_{cm}(t)/\sqrt{2}, \tag{19}$$

where

$$\Xi = \int_{-\infty}^{\infty} \psi_0(y, x_{cm}) A'(x_{cm}, y) dy. \tag{20}$$

Here $V^{eff}(x_{cm}, y)$ denotes the effective potential. Via Eq. (17), one gets the closed form expression for the equilibrium probability density $\psi_0(y, x_{cm})$. For the case $k > (-3x_{cm}^2 + 1)/2$, after some algebra one gets

$$\psi_0(y, x_{cm}) = \frac{e^{\frac{-2\theta^2 k - 8\theta y^2 - \frac{4y^4}{k}}{D}} \sqrt{\frac{2}{\theta k}}}{K\left[\frac{1}{4}, \frac{2\theta^2 k}{D}\right]}, \tag{21}$$

where K denotes the modified Bessel function of the second kind while $\theta = -1 + 2k + 3x_{cm}^2$. For large x_m, we have a more simplified $\psi_0(y, x_{cm})$:

$$\psi_0(y, x_{cm}) = e^{\frac{8(1-2k)y^2}{D}} \sqrt{\frac{-8 + 16k}{D\pi}}. \tag{22}$$

The effective potential energy

$$V^{eff}(x_{cm}) = \int_0^{x_{cm}} \Xi dx'_{cm} \tag{23}$$

$$= x_{cm}^4 + \frac{(3D + 16(1-2k)k)x_{cm}^2}{8k(-1+2k)} \tag{24}$$

have potential minima at $x_{cm} = x'_m = \pm(1)/(4)\sqrt{16 + (3D)/(k - 2k^2)}$ and potential maxima at $x_{cm} = 0$.

The effective barrier height ΔV_{eff} is the difference between the potential energies at the saddle point and the stable point $\Delta V_{eff} = V_{eff}(0) - V_{eff}(-x'_m)$. One gets

$$\Delta V_{eff} = \frac{(3D + 16(1-2k)k)^2}{256(1-2k)^2 k^2}. \tag{25}$$

Exploiting Eq. (25) one can see that ΔV_{eff} decreases as k increases from 1/2 to k_{min} where $k_{min} = (2 + \sqrt{4 + 6D})/8$. ΔV_{eff} is minimum at $k_{min} = (2 + \sqrt{4 + 6D})/8$. and for $k > k_{min}$, the effective potential increases with k. k_{min} is an increasing function of D.

The curvatures at the barrier top ω_0 and the well minima $\omega_{x'_m}$ are given by $\omega_0 = -4 - 3D/4k - 8k^2$ and $\omega_{x'_m} = 8 + 3D/2k - 4k^2$, respectively. The crossing rate for the dimer is explored in a high barrier limit $\Delta V^{eff} \gg k_B T$. In the limit $k \to \infty$, the R goes to the rate of globular dimer.

Before we evaluate the rate, let us first study how V^{eff} behaves as a function of x_{cm}. As shown in Fig. 9(a), the effective potential is indeed a double-well potential with two minima points. The rate as a function of coupling constant is plotted in Fig. 9(b). The figure exhibits that the rate monotonously decreases as k increases. As shown in the same figure, the rate from the adiabatic elimination approximation remarkably agrees with the numerical results.

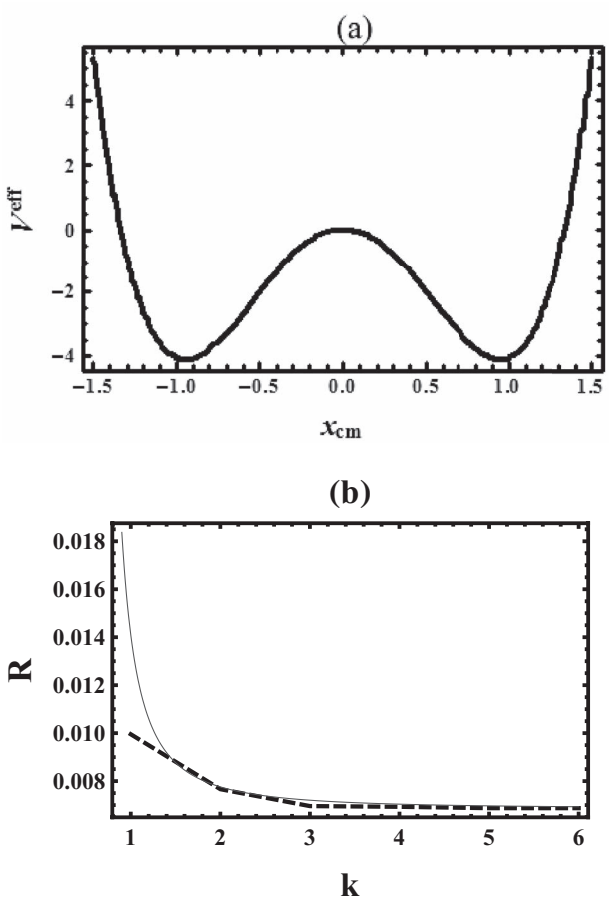

FIG. 9. (a) The effective potential as a function of x_{cm} for parameter choice $D = 0.4$ and $k = 8$. (b) Dimer crossing rate R as a function of coupling constant k for noise strength $D = 0.4$. The solid line shows the rate evaluated analytically from the adiabatic elimination approximation, while the dashed line indicates the rate from the numerical simulations.

VI. STOCHASTIC RESONANCE OF THE DIMER

In the presence of periodic external force, the system response to the external stimulation may depend on the flexibility of the dimer, shape of the potential profile, and on the strength of the noise. Next, we study the dependence of the stochastic resonance on these model parameters employing two state approximations for large coupling constant k.

In the presence of time varying signal $A_0 \cos(\Omega t)$, the Langevin equation that governs the dynamics is given by

$$\frac{dx_1}{dt} = -4k(x_1 - x_2) - \frac{\partial U(x_1)}{\partial x_1} + \bar{A}_0 \cos(\Omega t) + \xi_1(t), \tag{26}$$

$$\frac{dx_2}{dt} = -4k(x_2 - x_1) - \frac{\partial U(x_2)}{\partial x_2} + \bar{A}_0 \cos(\Omega t) + \xi_2(t). \tag{27}$$

The parameters $\bar{A}_0$ and Ω designate the amplitude and angular frequency, respectively. Here $\bar{A}_0 = A_0 x_m / U_0$. From now on for convenience the bar will be dropped.

Employing two state model approach,[21,22] two discrete states $x(t) = \pm x'_m$ are considered. Let us denote n_+ and n_- to be the probability to find the polymer segment in the right (x'_m) and in the left $(-x'_m)$ sides of the potential wells, respectively. In the presence time varying signal, the master equation

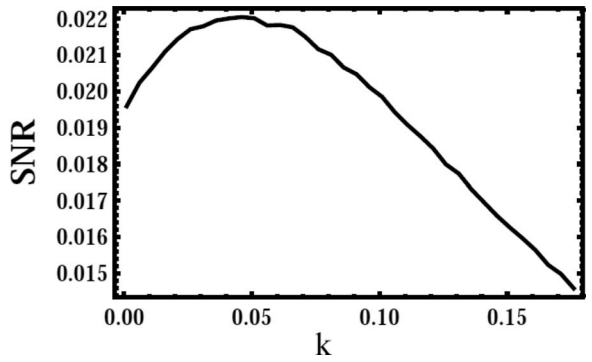

FIG. 10. (a) The dependence of *SNR* as a function of coupling constant k for noise strength $D = 0.2$ and amplitude $A_0 = 0.1$. The figure exhibits that the *SNR* increases as k increases and attains an optimal value at an optimal elastic constant k_{opt}. The optimal coupling constant shifts to the right as D increases.

that governs the time evolution of $n_\pm$ is given by

$$\dot{n}_\pm(t) = -(W_+(t) + W_-(t))n_\pm + W_\pm(t), \tag{28}$$

where $W_+(t)$ and $W_-(t)$ corresponds to the time dependent transition probability towards the right (x'_m) and the left $(-x'_m)$ sides of the potential wells. The time dependent rate takes a simple form

$$W_\pm = Rexp\left[\pm\frac{2}{D}A_0\cos(\Omega t)\right], \tag{29}$$

where R is the Kramers rate for the dimer's center of mass in the absence of periodic force $A_0 = 0$. For sufficiently small amplitude, one finds the signal noise ratio

$$SNR = \pi R\left(\frac{2A_0}{D}\right)^2. \tag{30}$$

The rate R is evaluated via numerical simulation.

For the dimer with a finite coupling constant k, the resonance behavior of the system is examined as shown in Fig. 10(a). The figure depicts that the *SNR* as a function of k for fixed $D = 0.2$ and $A_0 = 0.1$. For small k, the monomers tend to be non-interacting as a result the *SNR* becomes very small. The *SNR* peaks at an optimal coupling strength and then further increasing in k leads again to a smaller *SNR* as the rigid dimer is not flexible enough to adjust itself with the time varying force. The optimal spring constant increases as D steps up which is in agreement with the previous theoretical investigations.[10,11]

VII. SUMMARY AND CONCLUSION

In this paper, we have applied both numerical and analytical approaches to determine the escape rate of a dimer crossing a potential barrier. We find that for small k the statistics of the dimer can be well approximated by a three state Markov scheme. By computing the rates of this scheme we show that the escape rate of the dimer is a nonomontonic function of k peaked at an optimal coupling strength k_{opt}. This result demonstrates that cooperativity has a nontrivial effect on the escape rate of molecules. If cooperativity is too large then the escape rate of the dimer is reduced since both monomers will have to cross the barrier roughly simultaneously. Also, if cooperativity is absent then the escape rate is small since both monomers behave independently, i.e., the barrier crossing of one monomer does not influence the crossing of the other. Our essential finding here is that at an optimal degree of cooperativity the escape rate of a dimer is maximized. This result may have direct relevance to biological molecules, such as Kinesin, which has a structure that can be well approximated by a dimer. In effect, we have shown that the reaction rate of this molecule can be optimized by tuning the force of interaction between the heads (or lobes) of the molecule. It will be interesting to explore further if proteins, with dimer like properties, utilize this property to control and optimize their reaction rates.

Our results in this paper can potentially have applications to the study of transport of biological molecules. In effect, we have shown that the mobility of a protein with a dimeric structure will be crucially sensitive to the strength of interaction of the heads (or lobes) of the molecule. Perhaps the best example of an important biological molecule is Kinesin, which is responsible for intracellular transport along microtubules. The structure of Kinesin is known to be composed primarily of two heavy chains (or lobes) which are responsible for the catalytic binding and unbinding to the microtubule tracks. These two domains are linked by a small peptide referred to as the neck linker. In several elegant studies it was shown that the transport of Kinesin is crucially sensitive to the precise molecular structure of the neck linker.[28–30] In fact, in an elegant study Thorn *et al.* showed[29] that the mobility of a Kinesin molecule can be modulated by changing the total charge of the neck linker. The authors further argued that modulating the electrostatic interactions within the linker changes the cooperativity of the lobes, which directly influences the mobility of Kinesin. Interestingly, these experimental results support our finding that the transport properties of a dimer are sensitive to the strength of interaction of the two lobes. In fact, it is very likely that modulating the charge of the neck linker will have direct influence on its stiffness, which can potentially be modeled by an effective spring constant k. However, further analysis will have to be done to justify the reduction of a complex biological molecule, such as Kinesin, to the simple two particle problem considered here. Nevertheless, our work will serve as a starting point to explore systematically how the geometry of a molecule influences its transport and reaction rates.

The results of this paper indicate that there is a direct relationship between the flexibility of a macromolecule and its transport properties. Hence, we expect that in general this relationship can be applied to control the transport of molecules by modulating their flexibility. Modifying the flexibility of a macromolecule can be achieved in a variety of ways. For example, it is well known that the flexibility of proteins can be altered by ligand binding (for example, see Ref. 31). Also, numerous studies have demonstrated that the elasticity of DNA can be controlled by introducing external charges which change the electrostatic interactions between the two helixes.[32] Furthermore, it is well known that thermal and chemical denaturation dramatically increases the flexibility of biological molecules. This occurs because of hydrogen bond breaking which leads to an increase in the rotational

degrees of freedom of atoms and therefore increases the macroscopic flexibility of the molecule.[33,34] Using this approach it is likely that macromolecules with desired transport properties can be fabricated by manipulating their flexibility.

The transport and response properties of macromolecules are difficult to understand due to the structural complexity of these systems. The current study will serve as a useful starting point to understand these systems since a dimer is essentially the simplest possible macromolecule. Thus, it is likely that our essential findings can be generalized to systems with several monomers or subunits. In particular, our study highlights the crucial role played by cooperativity between components, which is likely to be even more important in a multicomponent setting. Also, we expect that the dynamics of a macromolecule can be coarse grained to discrete states, in much the same way that a dimer can reduced to a three state model. Thus, our study will serve a guide in the construction of simplified Markov state models of these complex biological structures. However, much work needs to be done to understand the statistical features of these systems. It will be interesting to explore this behavior, and to study its relevance to macromolecules with important biological relevance.

ACKNOWLEDGMENTS

We would like to thank Hiroshi Teramoto for discussion we had. M.A. would like to thank Professor W. Sung for interesting discussions he had during his visit at APCTP, South Korea. This work was supported in part by the National Heart, Lung, and Blood Institute (Grant No. R01HL101196).

APPENDIX: ADIABATIC ELIMINATION

One can rewrite Eq. (15) in different form

$$\frac{\partial}{\partial t}P(x_{cm}, y, t) = (L_{cm}(x_{cm}, y) + kL_y(y, x_{cm})), \quad \text{(A1)}$$

where

$$L_{cm}(x_{cm}, y) = \frac{\partial}{\partial x_{cm}}A'(x_{cm}, y) + \frac{1}{2}D\frac{\partial^2}{\partial x_{cm}^2}, \quad \text{(A2)}$$

$$L_y(y, x_{cm})) = -\frac{\partial}{\partial y}B'(y, x_{cm}) + \frac{1}{2}D\frac{\partial^2}{\partial y^2}. \quad \text{(A3)}$$

The eigenfunction of the operator L_y is $\psi_n(y, x_{cm})$, where $L_y\psi_n(y, x_{cm}) = -\lambda_n\psi_n(y, x_{cm})$. We have a stationary solution $\psi_n(y, x_{cm}) = P_{st}(y, x_{cm})$, $\lambda_0 = 0$. The eigenfunction $\psi_n^+(y, x_{cm})$ of the adjoint operator L_y^+ satisfies the relation $L_y^+\psi_n^+(y, x_{cm}) = -\lambda_n\psi_n^+(y, x_{cm})$. ψ_n^+ and ψ_n satisfy the orthogonality and completeness relation. We now expand the distribution function $P(x_{cm}, y, t)$ in terms of the complete set of ψ_n of the operator L_y as $P(x_{cm}, y, t) = \sum_{m=0}^{\infty} C_m(x_{cm}, t)\psi_m(y, x_{cm})$. Inserting this equation into Eq. (31) and multiplying with ψ_n^+ and integrating over y leads

$$\left(\frac{\partial}{\partial t} + k\lambda_n\right)C_n = \sum_{m=0}^{\infty} C_m L_{n,m}, \quad \text{(A4)}$$

which is exact. Here the operator $L_{n,m}$ with respect to x_{cm} has a form $L_{n,m} = \int \psi_n^+ L_{cm}\psi_m dy$. The adiabatic elimination of fast variable is valid when k is large. We have two main time scales; i.e, the slow dynamics which is governed by the center of mass motion and the fast time changing motion (the relative motion y). Utilizing the eigenfunction expansion method,[26,27] for large k, one finally gets

$$\frac{\partial}{\partial t}C_0 = L_{0,0}C_0 + \frac{1}{k}\sum_{n=1}^{\infty} L_{0,n}\frac{1}{\lambda_n}L_{n,0}C_0. \quad \text{(A5)}$$

One can note that $C_0(x_{cm}, t) = \int P(x_{cm}, y, t)dy = P_0(x_{cm}, t)$ and

$$L_{0,0} = \frac{\partial}{\partial x_{cm}}\bar{A}(x_{cm}, y) + \frac{1}{2}\bar{D}\frac{\partial^2}{\partial x_{cm}^2}, \quad \text{(A6)}$$

where $\bar{A}(x_{cm}, y) = \int A'(x_{cm}, y)\psi_0 dy$ and $\bar{D} = \int D\psi_0 dy = D$. For large k, the dynamics of the center is examined by considering first order approximation. Hence, Eq. (34) has simplified Fokker–Planck equation

$$\frac{\partial}{\partial t}P_0(x_{cm}, t) = \left\{\frac{\partial}{\partial x_{cm}}\int A(x_{cm}, y)\psi_0(y, x_{cm})dy\right\} \times P_0(x_{cm}, t) + \frac{1}{2}D\frac{\partial^2}{\partial x_{cm}^2}P_0(x_{cm}, t) \quad \text{(A7)}$$

which is the same as Eq. (18).

[1] P. Hänggi, P. Talkner, and M. Borkovec, Rev. Mod. Phys. **62**, 251 (1990).
[2] K. L. Sebastian and A. Debnath, J. Phys. Condens. Matter **18**, S283 (2006).
[3] P. J. Park and W. Sung, J. Chem. Phys. **111**, 5259 (1999).
[4] S. Lee and W. Sung, Phys. Rev. E **63**, 021115 (2001).
[5] F. Marchesoni, C. Cattuto, and G. Costantini, Phys. Rev. B **57**, 7930 (1998).
[6] K. L. Sebastian and A. K. R. Paul, Phys. Rev. E **62**, 927 (2000).
[7] J. F. Lindner, B. K. Meadows, W. L. Ditto, M. E. Inchiosa, and A. R. Bulsara, Phys. Rev. Lett. **75**, 3 (1995); Phys. Rev. E **53**, 2081 (1996).
[8] F. Marchesoni, L. Gammaitoni, and A. R. Bulsara, Phys. Rev. Lett. **76**, 2609 (1996).
[9] I. E. Dikshtein, D. V. Kuznetsov, and L. Schimansky-Geier, Phys. Rev. E. **65**, 061101 (1996).
[10] M. Asfaw and W. Sung, EPL **90**, 3008 (2010).
[11] M. Asfaw, Phys. Rev. E **82**, 021111 (2010).
[12] P. Jung, U. Behn, E. Pantazelou, and F. Moss, Phys. Rev. A **46**, R1709 (1992).
[13] A. Pototsky, F. Marchesoni, and S. E. Savelevl, Phys. Rev. E **81**, 031114 (2010).
[14] A. Pototsky, N. B. Janson, F. Marchesoni, and S. E. Saveleva, Chem. Phys. **375**, 458 (2010).
[15] E. Heinsalu, M. Patriarca, and F. Marchesoni, Phys. Rev. E **77**, 021129 (2008).
[16] O. M. Braun, R. Ferrando, and G. E. Tommei, Phys. Rev. E **68**, 051101 (2003).
[17] C. Fusco, A. Fasolino, and T. Janssen, Eur. Phys. J. B **31**, 95 (2003).
[18] I. Derenyi and T. Vicsek, Proc. Natl. Acad. Sci. U.S.A. **93**, 6775 (1996).
[19] P. S. Burada, G. Schmid, D. Reguera, M. H. Vainstein, J. M. Rubi, and P. Hänggi, Phys. Rev. Lett. **101**, 130602 (2008).
[20] R. Benzi, G. Parisi, A. Sutera, and A. Vulpiani, Tellus **34**, 10 (1982).
[21] L. Gammaitoni, P. Hänggi, P. Jung, and F. Marchesoni, Rev. Mod. Phys. **70**, 223 (1998).
[22] B. McNamara and K. Wiesenfeld, Phy. Rev. A **39**, 4854 (1989).
[23] E. Heinsalu, M. Patriarca, and F. Marchesoni, Chem. Phys. **375**, 410 (2010).
[24] I. Goldhirsch and Y. Gefen, Phys. Rev. A **33**, 2583 (1986).
[25] I. Goldhirsch and Y. Gefen, Phys. Rev. A **35**, 1317 (1987).
[26] K. Kaneko, Prog. Theor. Phys. **66**, 129 (1981).
[27] H. Risken, *The Fokker-Planck Equation: Methods of Solution and Applications*, 2nd ed. (Springer-Verlag, Berlin/Heidelberg, 1989).

[28]R. B. Case, S. Rice, C. L. Hart, B. Ly, and R. D. Vale, Curr. Biol. **10**, 157 (2000).
[29]K. S. Thorn, J. A. Ubersax, and R. D. Vale, J. Cell Biol. **151**, 1093 (2000).
[30]M. Tomishige and R. D. Vale, J. Cell Biol. **151**, 1081 (2000).
[31]R. l. Najmanovich, J. Kuttner, V. Sobolev, and M. Edelman, Proteins: Struct., Funct., Genet. **39**, 261 (2000).
[32]A. Podest, M. Indrieri, D. Brogioli, G. S. Manning, P. Milani, R. Guerra, L. Finzi, and D. Dunlap, Biophys. J. **89**, 2558 (2005).
[33]B. Schulze, A. Sljoka, and W. Whiteley, AIP Conf. Proc. **1368**, 135 (2011).
[34]B. M. Hespenheid, A. J. Rader, M. F. Thorpe, and L. A. Kuhn, J. Mol. Graphics Modell. **21**, 195 (2002).